AGU PUBLICATIONS

JGR

Journal of Geophysical Research: Atmospheres

RESEARCH ARTICLE

10.1002/2014JD021616

Key Points:
- Spherical models are unable to represent the radiative properties of snowflakes
- Radiative properties of snowflakes should be modeled with advanced techniques
- The realistic modeling of snow is important for large aggregated particles

Correspondence to:
D. Ori,
davide.ori3@unibo.it

Citation:
Ori, D., T. Maestri, R. Rizzi, D. Cimini, M. Montopoli, and F. S. Marzano (2014), Scattering properties of modeled complex snowflakes and mixed-phase particles at microwave and millimeter frequencies, *J. Geophys. Res. Atmos.*, *119*, 9931–9947, doi:10.1002/2014JD021616.

Received 7 FEB 2014
Accepted 24 JUL 2014
Accepted article online 30 JUL 2014
Published online 27 AUG 2014

Scattering properties of modeled complex snowflakes and mixed-phase particles at microwave and millimeter frequencies

D. Ori[1,2], T. Maestri[2], R. Rizzi[2], D. Cimini[3,4], M. Montopoli[4,5], and F. S. Marzano[4,5]

[1]Department of Biological, Geological and Environmental Sciences, University of Bologna, Bologna, Italy, [2]Department of Physics and Astronomy, University of Bologna, Bologna, Italy, [3]Institute of Methodologies for the Environmental Analysis, National Research Council of Italy, Potenza, Italy, [4]Center of Excellence CETEMPS, University of L'Aquila, L'Aquila, Italy, [5]Department of Information Engineering,University of Rome La Sapienza, Rome, Italy

Abstract A microphysically based algorithm (named Snow Aggregation and Melting (SAM)) that models snowflakes composed of a collection of hexagonal columns by simulating a random aggregation process is presented. SAM combines together pristine columns with multiple dimensions to derive complex aggregates constrained to size-mass relationship obtained by data collected from in situ measurements. The model also simulates the melting processes occurring for environmental temperatures above 0°C and thus define the mixed-phase particles structure. The single-scattering properties of the modeled snowflakes (dry and mixed phased) are computed by using a discrete dipole approximation (DDA) algorithm which allows to model irregularly shaped targets. In case of mixed-phased particles, realistic radiative properties are obtained by assuming snow aggregates with a 10% of melted fraction. The single-scattering properties are compared with those calculated through Mie theory together with Maxwell-Garnett effective medium approximation using both a homogeneous sphere and a layered-sphere models. The results show that for large-size parameters there are significant differences between the radiative properties calculated using complex microphysical and optical algorithms (i.e., SAM and DDA) and those obtained from simplified assumptions as the layered-sphere models (even when the radial ice density distribution of the aggregated snowflakes is perfectly matched). Finally, some applications to quantitative precipitation estimation using radar data are presented to show how the resulting differences in the basic optical properties would propagate into radar measurable. Large discrepancies in the derivation of the equivalent water content and snowfall rate from radar measurements could be observed when large-size parameters are accounted for.

1. Introduction

Remote sensing measurements are the only practical means for achieving a global coverage of precipitation phenomena. The interpretation of remote sensing data relies, in part, on the microphysical description of the hydrometeors, capable to simulate the complex snowflakes physical properties, and on the modeling of their single-scattering radiative properties through realistic assumptions concerning the ice crystal habits and mass distribution.

Due to the high degree of the complexity of the problem, nonspherical ice crystals and snow aggregates have commonly been modeled, for radar and passive microwave (MW) radiative transfer purposes, as spheres or alternatively spheroids composed of a homogeneous mixture of air and ice [*Korolev et al.*, 2003; *Matrosov*, 2007]. These simplified models, commonly named soft-spheroid models, have reached a large popularity due to the associated exploitation of scattering numerical methods, such as the T-Matrix or TMM [*Mishchenko et al.*, 1996], that allow to compute an analytical solution within short computational times. Nonetheless, the simplified assumption, concerning the shape of complex ice crystal, has been recognized to be one of the main sources of error in the retrieval of snowfall from remote sensing measurements [*Kulie et al.*, 2010].

Field observations of snow particles [*Locatelli and Hobbs*, 1974] show that aggregates have densities that are dependent on particle dimensions (the smaller the particle, the denser it is). This suggests that the inner parts of a large snowflake are denser than the outer ones. Thus, it is reasonable to interpret snowflakes as particles with density that decreases from the center to the edges. At this regard the inadequacy of the

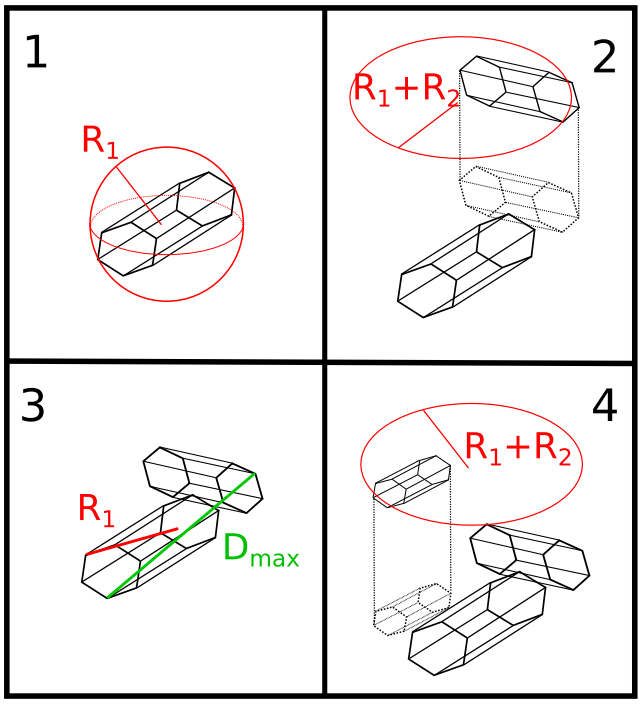

Figure 1. The aggregation scheme in four steps (from left to right). The geometrical properties of the aggregate R and D_{max} are plotted respectively with a red and a green line. In the second and fourth panel the total circular area containing the geometrical cross section of the joint CAP and NAP is shown.

soft-spheroid models to represent complex snowflakes is evident since, for these methods, ice particles can only be assumed to have a uniform density. Recent studies [*Ishimoto*, 2008; *Botta and Aydin*, 2010; *Petty and Huang*, 2010; *Tyynela et al.*, 2011], developed by performing computations based on accurate scattering models, have demonstrated that models assuming spherically/spheroidally shaped snow particles are unable to properly represent the peculiar radiative characteristics of snowflakes, especially when the incident wavelength is of the same order of magnitude of the particle size. It appears that snowflakes should be represented as complex aggregates of pristine ice crystals, and thus, we must rely on advanced and nonanalytical methods for the computation of the radiative properties. Recent studies have also attempted the development of optimal retrieval algorithms for snow characteristics from active/passive sensors synergy [*Löhnert et al.*, 2011] and have investigated the sensitivity of ground-based passive MW measurements in the frequency range 22–150 GHz to snowfall characteristics [*Kneifel et al.*, 2010]. However, these experimental analyses report the lack of single-scattering databases for large snow aggregates (>1 cm) at MW frequencies up to 150 GHz.

The two most commonly used methods to compute the single-scattering properties of complex particles are the finite difference time domain [*Taflove and Hagness*, 2005] and the discrete dipole approximation (DDA) [*Draine*, 1988]. Among others, scattering properties of multiple sets of pristine ice particle shapes obtained through DDA have been presented by *Evans and Stephens* [1995], *Liu* [2004, 2008a], *Kim et al.* [2007], *Hong* [2007a], and *Grecu and Olson* [2008]. *Hong* [2007b] studied a simple aggregate of hexagonal prisms while the first application of the DDA to model snow aggregates was given by *Osharin* [1994]. *Petty and Huang* [2010] demonstrated, again by exploiting DDA calculations, the inadequacy of the soft-sphere approximation for representing the radiative properties of large aggregates at microwave frequencies. Analyzing colocated airborne radar measurements at 13.4 GHz, 35.6 GHz, and 94 GHz, *Leinonen et al.* [2012] provided empirical evidences of the nonspheroidal behavior of the snow backscattering properties.

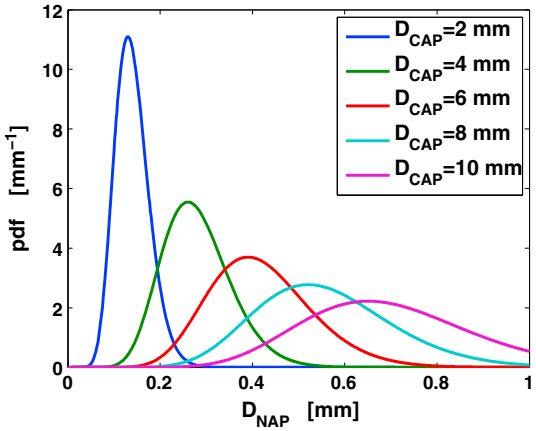

Figure 2. Evolution of the probability density functions of the size of the NAP for increasing maximum dimension of the CAP.

The correct representation of the single-scattering properties of snow aggregates is fundamental for the implementation of an accurate precipitation retrieval algorithm. Therefore, a physically based model describing the complex structure of realistic snowflakes is needed, and this work aims at providing a possible solution by constraining the microphysical properties of the hydrometeors to measured size-mass relations.

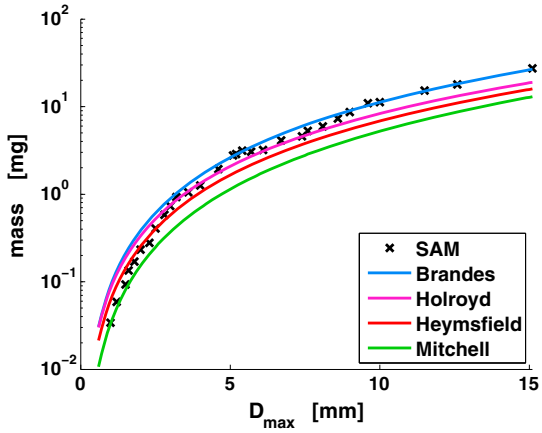

Figure 3. Aggregate mass as a function of the size. The colored curves represent multiple size-mass relations derived from measured data: *Brandes et al.* [2007] (blue), *Holroyd* [1971] (magenta), *Heymsfield et al.* [2004] (red), and *Mitchell* [1996] (green). Black crosses are the values of the simulated aggregates.

A very recent study [*Nowell et al.*, 2013] calculates the radiative properties of realistic snowflakes modeled as fractal structures following a predefined mass-size relationship. They also compare the radiative properties computed with DDA with those of spherical targets of equivalent mass computed with Mie theory. The model of Nowell et al. simulates the random growth of a fractal aggregate in a cubic lattice domain using a very simplified six-bullet rosette as constitutive pristine crystal (a rosette is composed of only 13 lattice points when its maximum dimension is equal to 0.2 mm and only 19 when its maximum dimension is 0.4 mm). All the crystals in the aggregate have the same orientation with respect to the reference frame; nevertheless, the model allows to control the size, mass, aspect ratio, and fractal dimension of the resulting aggregate.

The present paper introduces an aggregation algorithm based on the physics of collision-coalescence of realistically shaped hexagonal columns. The snowflake microstructure is described through realistic constitutive particles (hexagonal columns) that are free to assume any orientation in space. Moreover, an accurate description of the pristine crystals geometry is given. Since a cubic lattice grid of 20 μm is used for the DDA computations, the minimum dimension of the pristine hexagonal columns is represented by at least five dipoles (in Nowell et al. the branch of the bullet rosettes consist of a single dipole). The finer resolution of the lattice domain implies more accurate DDA computations. Results from SAM-DDA model are compared to results obtained using a soft-sphere model (ice density is assumed homogeneous) and two layered-sphere models (with ice density varying within the spherical volume). The soft- and layered-sphere models are used in combination with Mie theory in order to derive radiative properties to be used as reference.

Section 2 describes the different microphysical models and in particular the innovative SAM methodology. In section 3 the results of the scattering computation applied to the microphysical models are presented. In the last section (4) the conclusions are drawn.

2. Hydrometeors Modeling

Different microphysical models are considered in this paper to evaluate the effect of shape, mass distribution, and size-mass relation on the single-scattering properties and main radar parameters in presence of snowflakes. The models' configurations are as follows: (1) the SAM model applied to ice aggregates,

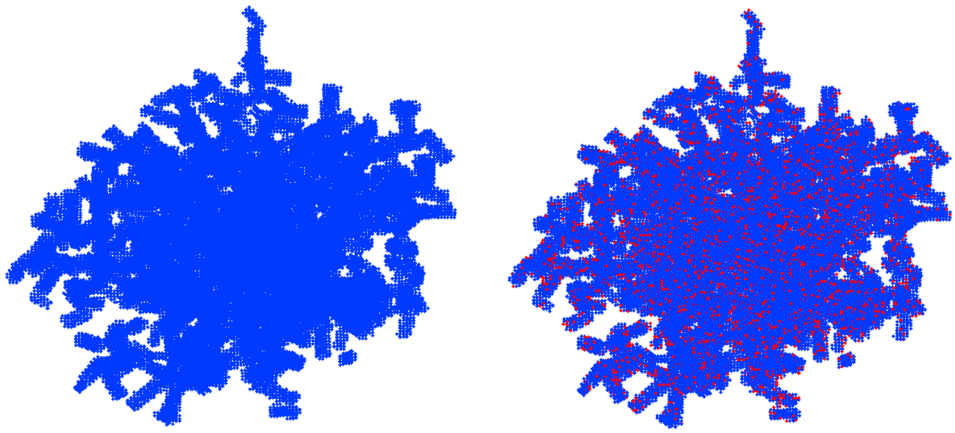

Figure 4. Image of a dry aggregate snowflake with (left) $D_{max} = 3$ mm. (right) The same aggregate with 10% of melted mass (red dots).

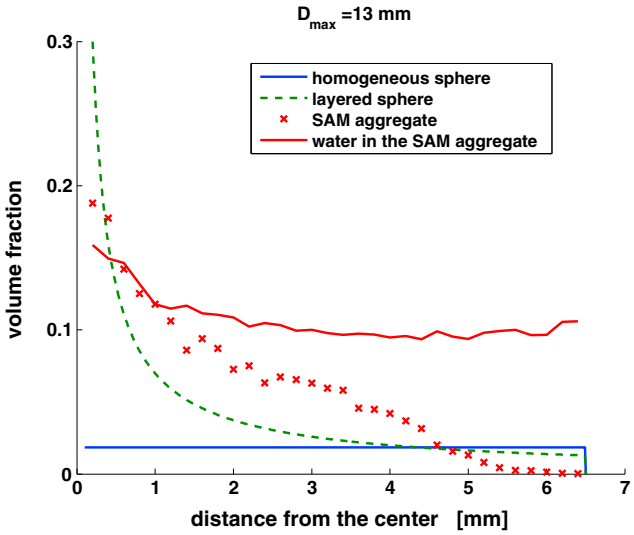

Figure 5. Volume fraction (ratio between mass density and ice mass density) as a function of the distance from the center of mass of the snowflake for an aggregate with maximum dimension of 13 mm. The volume fraction radial distribution is plotted for homogeneous sphere (blue), layered sphere (dotted green), and SAM aggregate (red crosses) models. The figure also shows the liquid water fraction (red line) for the corresponding partially melted snowflakes. In order to calculate the effective density of the aggregate models (SAM), the space is divided in spherical shells of equal thickness (0.2 mm) and the number of dipoles belonging to each spherical shell are counted. The water fraction is computed dividing the number of water dipoles in each shell by the total number of dipoles belonging to that shell.

(2) SAM applied to partially melted snowflakes (3) the soft-sphere model (4) the layered-sphere model, and (5) the layered-sphere model that exactly maps the radial mass distribution of SAM aggregates. The soft- and layered-sphere models will be only briefly described since they are widely known to the scientific community and are used here as reference, whereas the innovative SAM model will be illustrated in detail.

2.1. SAM: Aggregation Model for Dry Particles

An innovative algorithm, called Snow Aggregation and Melting (SAM), is developed to model the aggregation of snowflakes. SAM generates complex shapes by randomly aggregating pristine ice crystals. For this work, hexagonal columns are selected as the basic shape that composes the aggregates in accordance with studies [i.e., *Magono and Lee*, 1966] reporting that one of the basic habit of the ice crystal within clouds is the hexagonal column. A realistic internal mass distribution is obtained by clustering particles with increasing dimension as the maximum size of the aggregate increases.

The SAM algorithm sequence is described by four steps that are graphically represented in Figure 1.

1. First, the geometrical properties of a hexagonal column are defined. Its center of mass is placed in the origin of the coordinate system. R_1 is the radius of the smallest sphere centered in the center of mass of the crystal that encloses the whole particle. In case of a hexagonal prism, R_1 is simply the distance from a prism vertex to its center of mass. The crystal is then randomly rotated around its three Cartesian axes. The whole aggregation process starts around this basic shape that is the core around which the full aggregate is constructed and for that reason is here referred as the core aggregation particle (CAP) (first panel of Figure 1).
2. The geometrical properties of a second hexagonal prism (the next adding particle, NAP) are defined. The radius of the smallest sphere enclosing it, hereafter noted as R_2, is calculated. This particle is randomly rotated around its axes. The NAP is positioned above the CAP with its center of mass randomly placed in the area defined by a cross section of magnitude given by $\pi(R_1 + R_2)^2$ and centered around the z axis. The NAP is afterward forced to fall until it touches the CAP. If the contact occurs, the two particles stick together and a new CAP is generated. If the particles do not touch each other, the method repeats the descent of the NAP toward the CAP but with a different randomly defined configuration (second panel, Figure 1) until a contact occurs.
3. The new CAP center of mass is placed at the origin of the coordinate system, R_1 is updated, and D_{max} (the diameter of the smallest sphere enclosing the whole particle) is calculated. If D_{max} exceeds an established limit value, the aggregation process stops (third panel, Figure 1).
4. If the established value D_{max} is not reached, the model proceeds as described at points (2) and (3) and a new pristine particle is added to the CAP (fourth panel).

The size of the NAP ($2R_2$) varies during the aggregation process and becomes larger as the aggregates maximum dimension (D_{max}) increases. The NAP dimension is, in fact, extracted randomly from a population of

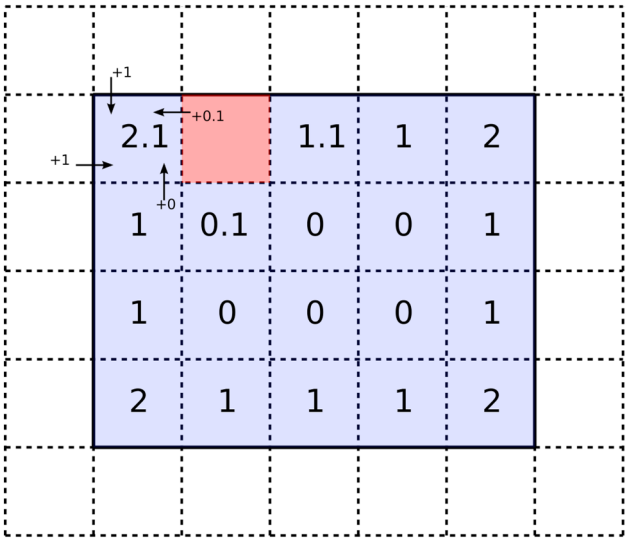

Figure 6. A two-dimensional representation of the technical procedure used to compute the melting probability. The color code for the type of material and phase of the lattice regions are as follows: blue for ice, red for water, and white for air. For each lattice region the melting probability is shown. As an example for the ice cell in the upper left corner the methodology that calculates the melting probability P_{tot} is specified.

hexagonal columns described by a gamma size distribution that evolves in accordance with the maximum size of the aggregate (CAP). The gamma distribution is defined as

$$f_{\theta,k}(x) = \frac{x^{k-1}e^{-x/\theta}}{\theta^k \Gamma(k)} \quad (1)$$

where k is the shape parameter, θ is the scale parameter, and $\Gamma(k)$ is the gamma function. The expected value and the variance of $f(x)$ are respectively $E[x] = k\theta$ and $V[x] = k\theta^2$. In our model we assume that both these parameters vary linearly with the aggregate maximum dimension so that

$$E[x] = k\theta = A \cdot D_{max} \quad V[x] = k\theta^2 = B \cdot D_{max} \quad (2)$$

where A and B are constants to be defined. A graphical representation of the evolution of the size distribution of the NAP is given in Figure 2. The two constants A and B are determined so that the final aggregate fits the available data concerning snowflakes size-mass relation and in particular that proposed by *Brandes et al.* [2007] that is here reported:

$$m(D_{max}) = 8.9 \cdot 10^{-5} \cdot D_{max}^{2.1} \quad (3)$$

The particle dimension D_{max} is in millimeters and its mass m is in grams. Figure 3 shows the evolution of the mass of the simulated aggregates for $A = 0.07$ and $B = 1$ mm as a function of their maximum dimension. The SAM solution is compared with the Brandes size-mass relation and with other relationships found in literature. Note that the SAM solution falls within the spread of the measured relations except for the lowest-particle dimensions. Equation (3) has been derived by Brandes as a least squares fit applied to measured data. Because of the larger variability in the bulk density of small snowflakes, the Brandes relation, obtained through a data interpolation process, best represents the microphysical properties of large particles while representation of the densities of very small snowflakes is less accurate. As a consequence, the mass value of the aggregated particle simulated by SAM with maximum dimension smaller than 3 mm is lower than the mass calculated through equation (3). Since the shapes of the largest particles are obtained by aggregating additional crystals to an agglomerate of smaller ones, equation (3) not only represents the mass of the aggregate as a function of its size but also describes the mass distribution (density) within each particle. An example of simulated snow aggregate is given in Figure 4 (left).

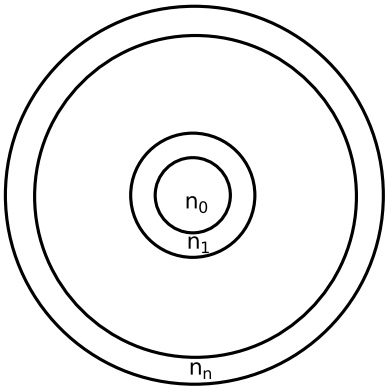

Figure 7. Scheme of a layered-sphere model. In our simulations the number of layers is $n = 500$ for the Mie-500 configuration and $n = 50$ for the Mie-SAM configuration (see text for details). All the layers have the same thickness.

Some important physical and geometrical characteristics such as the radial density distribution and the aspect ratio of the aggregates are briefly analyzed. Figure 5 shows the ratio between mass density and the mass density of pure ice (0.917 g/cm^3), as a function of the distance from the center, of a SAM aggregate with maximum dimension equal to 13 mm. The result obtained for the SAM aggregate is compared

Table 1. Microwave Frequencies and Dielectric Properties Used for Scattering Calculations

MW Band	Temp [°C]	*n* Water	*n* Ice	ϵ Water	ϵ Ice
C 5.6 GHz	0	8.34 + i2.22	1.79 + i7.76e-4	6.46e1 + i3.71e1	3.19 + i6.28e-4
	−40		1.77 + i1.16e-5		3.15 + i2.54e-4
X 9.6 GHz	0	7.20 + i2.85	1.79 + i2.65e-4	4.38e1 + i4.10e1	3.19 + i9.46e-4
	−40		1.77 + i1.22e-4		3.15 + i4.34e-4
Ku 13.6 GHz	0	6.28 + i3.01	1.79 + i3.62e-4	3.04e1 + i3.78e1	3.19 + i1.29e-3
	−40		1.77 + i1.73e-4		3.15 + i6.14e-4
Ka 35.6 GHz	0	4.04 + i2.42	1.79 + i9.18e-4	1.05e1 + i1.96e1	3.19 + i3.28e-3
	−40		1.77 + i4.52e-4		3.15 + i1.61e-3
W 89 GHz	0	2.93 + i1.48	1.79 + i2.41e-4	6.40 + i8.68	3.19 + i8.17e-3
	−40		1.77 + i1.19e-3		3.15 + i4.02e-3
W 94 GHz	0	2.89 + i1.43	1.79 + i2.41e-4	6.30 + i8.28	3.19 + i8.63e-3
	−40		1.77 + i1.19e-3		3.15 + i4.25e-3
157 GHz	0	2.59 + i1.05	1.79 + i4.04e-3	5.60 + i5.47	3.19 + i1.44e-2
	−40		1.77 + i2.00e-3		3.15 + i7.13e-3

to a homogeneous radial density distribution (soft-sphere model) and to a density distribution within a layered sphere following exactly equation (3). The radial mass distribution of the SAM aggregate follows the radial distribution derived from equation (3) with some expected discrepancies due to the random nature of the algorithm describing the aggregation process.

Brandes et al. [2007] defined the aspect ratio *ar* of the observed snowflakes as the ratio between the maximum vertical length and the maximum horizontal dimension measured by a two-dimensional video disdrometer. The aspect ratio is given as a function of the maximum dimension:

$$ar = 0.01714\, D_{\max} + 0.8467 \tag{4}$$

Equation (4) indicates that the flakes are nearly spherical (with mean values that increase from 0.84 at the smaller dimensions to about 1 at 10 mm).

Since the aggregates modeled by SAM do not account for any falling direction, *ar* values are calculated using a different methodology. For a given aggregated snowflake the major axis has been found. The second axis is the longest dimension in the orthogonal plane to the first axis. Finally, the third axis is the maximum dimension in the perpendicular direction to the plane defined by the other two axes. The aspect ratio value is calculated as the ratio of the minor axis to the major axis. Computed *ar* values for SAM aggregates range from 0.8 to 1. The results are consistent with the values found by *Brandes et al.* [2007].

2.2. SAM: Melting Model

The mixed-phase particles are derived by modeling a melting process similar to that discussed in *Fabry and Szyrmer* [1999]. They defined six different models describing partially melted hydrometeors composed of aggregates of ice crystals and water. *Korkmaz* [2004] exploited the six models to simulate radar signatures at S, X, and Ka bands and compared the results with data. He found that the best performance is achieved for the model of aggregates with the largest ice density near the core. According to these results, among the various configurations considered, it is the model of ice aggregate crystals covered by a thin layer of liquid water that performs best in representing measured radar parameters of partially melted hydrometeors. Moreover, laboratory observations of melting snowflakes, performed by *Oraltay and Hallett* [2005], suggest that the melting process starts from the high-curvature regions of the surface of the crystals.

Based on these results, the SAM model describes the melting process by starting from the ice phase aggregates derived in section 2.1. The dry and mixed-phase aggregates are described as clusters of polarizable regions belonging to a cubic lattice. A sequence of steps is performed to replace single ice lattice regions (points) with water ones. The aggregate mass is maintained constant during the whole process.

For each ice lattice point a probability of melting is defined. The not normalized probability associated to each single ice dipole *l* in the lattice structure of coordinates (x_l, y_l, z_l) is a function of the physical state (type of material and its phase) of the six regions surrounding it. This probability of melting is described mathematically in compact way by

$$P^l_{\text{tot}}(x_l, y_l, z_l) \propto \sum_{j,k} P_{\text{state}}(\mathbf{x}_l + j\mathbf{l}_k) \qquad j = -1, 1 \qquad k = 1, 2, 3 \tag{5}$$

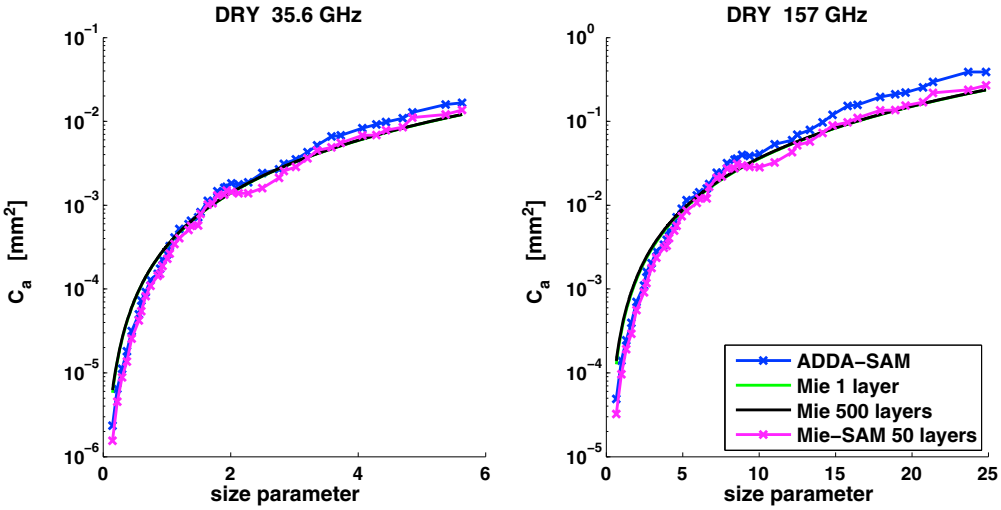

Figure 8. Total absorption cross section as a function of the maximum dimension of the particle for frequencies of 35.6 and 157 GHz.

where $\mathbf{I}_k$ is the kth row of the 3×3 identity matrix. Any lattice region might be composed of air, ice, or water (state index in equation (4)). Only the six regions that have a nonnull area of contact with the central region are accounted for in the computation of the melting probability of the central region in accordance with the Fourier's law of heat conduction. The SAM algorithm was run setting $P_{\text{air}} = 1, P_{\text{water}} = 0.1$, and $P_{\text{ice}} = 0$. A two-dimensional example of the computational scheme of the probability of melting associated at each dipole region is given in Figure 6.

The melting process algorithm statistically advantages the melting of the aggregate surface regions with respect to the inner parts of the particle since, at the initial steps, internal points, being surrounded only by other iced regions, have an associated probability to melt that is zero. The melting procedure is performed until the number of water regions reaches the value set by the user. For the present work a 10% of the total aggregate mass is water and the remaining is ice. The final configuration shows that the melted points are randomly distributed mostly on the particle surface (an example is given in Figure 4 (right)). The mixed-phase particle has the same mass and shape of the corresponding dry particle so that a direct comparison among the radar-derived parameters is possible. Since the natural melting process changes the morphology of the snowflake, this method is not appropriate to model mixed-phase particles with large

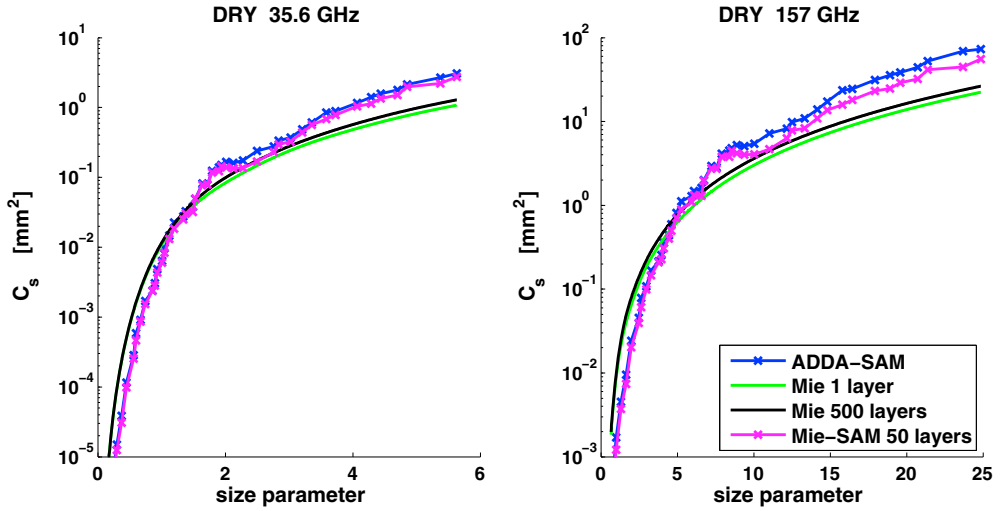

Figure 9. Total scattering cross section as a function of the maximum dimension of the particle for frequencies of 35.6 and 157 GHz.

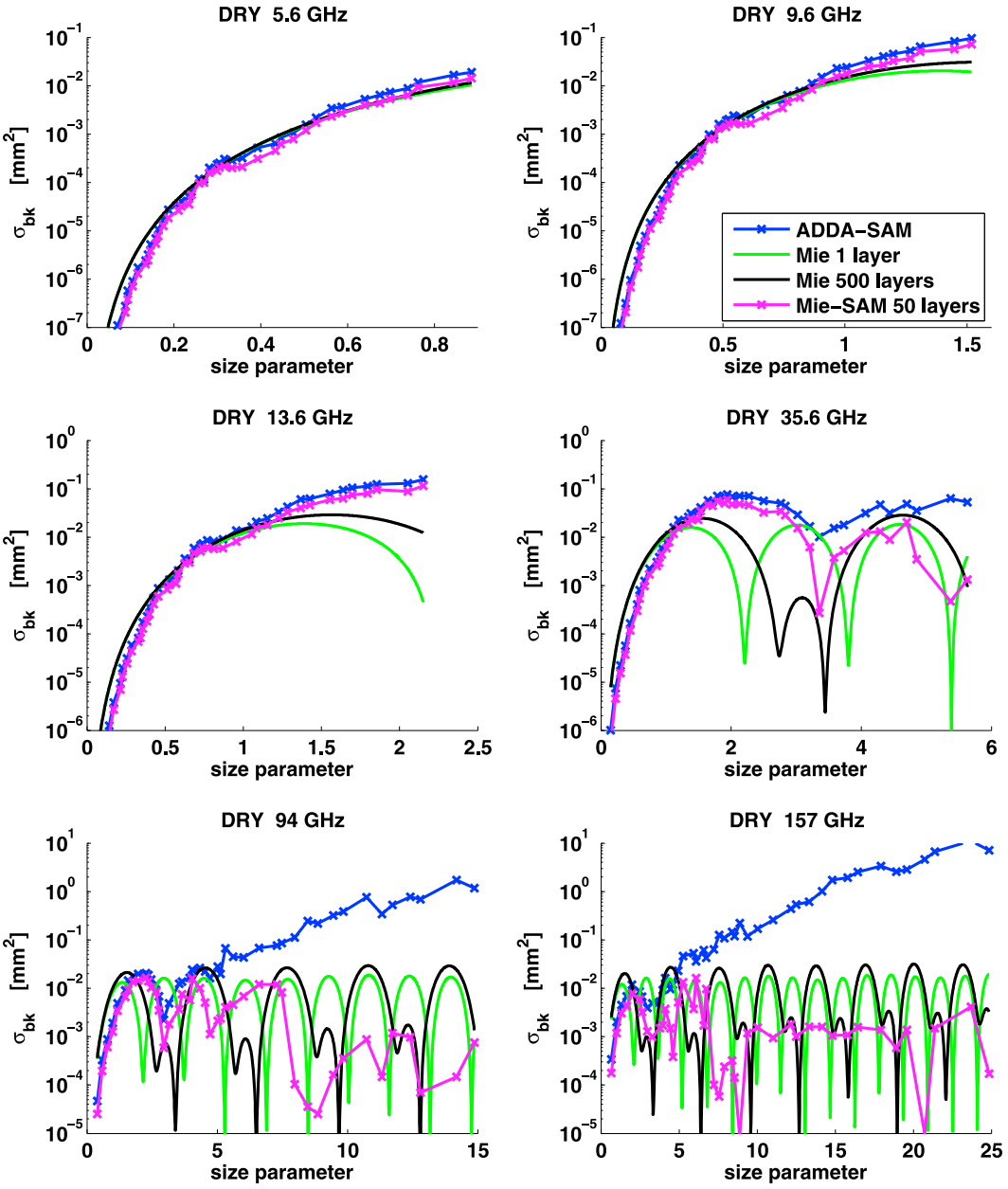

Figure 10. Radar backscattering cross section as a function of the size parameter of the particle for six different frequencies from 5.6 to 157 GHz. Results from Mie-1 homogeneous soft sphere (green), Mie-500 layered sphere (black), 50-layered Mie-SAM (magenta), and complex ADDA-SAM (blue) are compared.

values of melted fraction. However, Figure 4 shows that 10% of melted fraction covers just a small part of the total particle surface; thus, the use of the same shape in the computations is an acceptable assumption.

The melting fraction distribution inside a partially melted aggregate with maximum dimension of 13 mm is shown in Figure 5 by the red solid line. Details on the computation of the melted fraction are given in the figure caption. As expected values around 10% are encountered all along the aggregate's dimension. Slightly larger values are found near the core where the total particle density is very large due to the aggregation of small ice crystals; this is in accordance with *Fabry and Szyrmer* [1999].

2.3. Soft-Sphere Models

The simplest microphysical model relies on the assumption that snow particles are approximated by homogeneous spheres and the scattering properties are computed using the Mie analytical solution. These

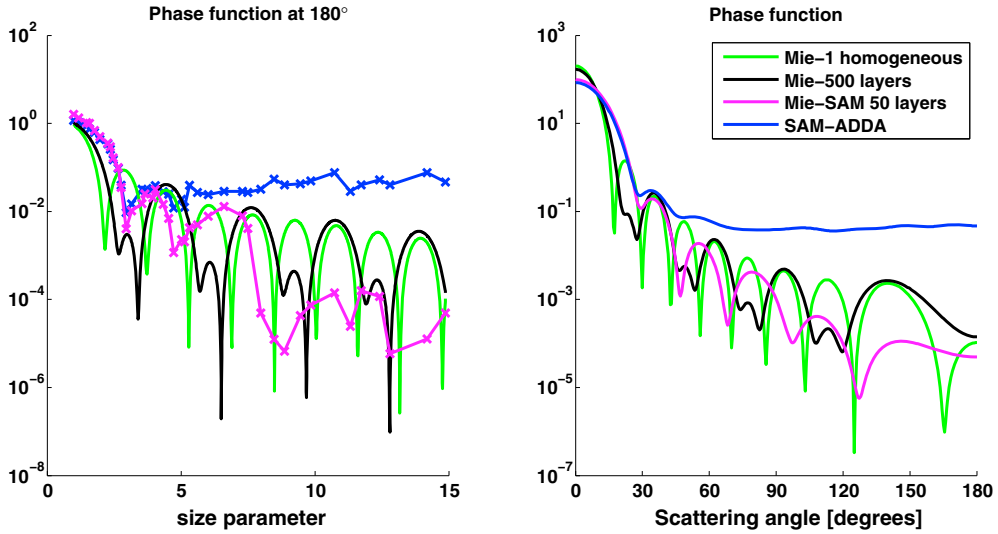

Figure 11. (left) Value of the phase function at 180° (backscattering) as a function of the particle maximum dimension at 94 GHz. (right) Phase function at 94 GHz of snowflakes with $D_{max} = 13$ mm. Results for ADDA-SAM (blue), homogeneous soft-sphere Mie-1 (green), Mie-500 layered sphere (black), and 50-layered Mie-SAM (magenta) models are shown.

models are commonly known as the soft-sphere models [*Liu*, 2004]. In this work the dielectric properties of the ice sphere are calculated using the Maxwell-Garnett mixing formula. The length of the sphere diameter is chosen to be equal to the maximum dimension of the corresponding aggregated particle. The soft-sphere model is also used to represent wet snowflakes. In this case a fraction of the ice mass is replaced with liquid water and the Maxwell-Garnett approximation is applied to the new mixture of three materials (water, ice, and air).

2.4. Layered-Sphere Models

A more complex model accounts for a core sphere surrounded by multiple shells. This type of geometrical model was developed to improve the modeling of radiative properties of nonhomogeneous particles accounting for a radially stratified structure [*Yang*, 2003]. We use the code developed by *Pena and Pal* [2009] with spherical layers with equal thickness (Figure 7). Each layer is characterized by a specific index of refraction computed using the Maxwell-Garnett mixing formula.

The layered-sphere model is run in two different configurations.

1. Mie-500. In this configuration it is assumed that the mass-size relation follows exactly equation (3) [*Brandes et al.*, 2007]. A number of 500 spherical shells are assumed. It is important to note that the choice of 500 layers allows to simulate a highly stratified sphere. Different numbers of layers have been tested, and no significant differences in the resulting radiative properties have been found for numbers larger than 50. Partially melted snowflakes are modeled by converting an equal fraction of ice mass into water for each layer. The Maxwell-Garnett formula is used to compute the effective dielectric constant of the mixture of ice, water, and air.
2. Mie-SAM model. In this configuration a 50-layer sphere model with the exact radial mass distribution of the aggregates modeled by SAM is assumed. This allows a better comparison with the results obtained using the SAM algorithm that does not perfectly follows equation (3). In case of mixed-phase particles the same distribution of melted fraction of mixed-phase aggregates is used.

3. Results

3.1. Scattering Codes and Methodology

Simulated single-scattering properties of snowflakes are presented for seven typical radar frequencies (first column of Table 1). The refractive indices used in the computations (Table 1) are derived from the model of *Meissner and Wentz* [2004] for pure water at 0°C and from the *Matzler* [2006] model for ice at −40°C and 0°C.

Scattering computation of the homogeneous sphere and of the layered soft-sphere models are performed using respectively a standard Mie code and the *scattnlay* code by *Pena and Pal* [2009]. Scattnlay is a publicly

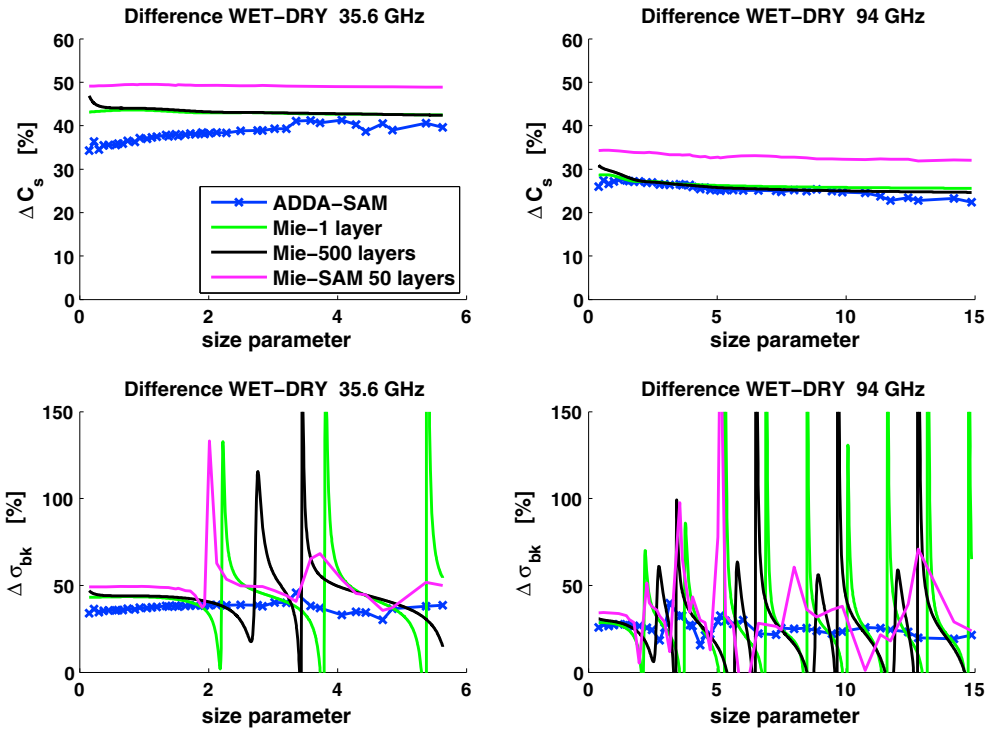

Figure 12. Differences in the (top row) total scattering and (bottom row) backscattering cross sections between wet and dry snowflakes as a function of the maximum dimension of the particles. Results are for (left column) Ka band and (right column) W band.

available implementation of the algorithm for the calculation of the Mie scattering coefficients of a multilayered sphere developed by *Yang* [2003]. The dielectric properties of mixtures of materials are computed using the Maxwell-Garnett mixing formula. In the case of dry snowflakes ice is considered inclusion in air matrix, while for mixed-phase particles water is considered inclusion in ice matrix and as a second interaction the ice-liquid water mixture is considered as inclusion in air matrix. The dielectric mixing formula of Bruggeman and that of Sihvola [*Petty and Huang*, 2010] have also been tested. The discrepancies between the resulting radiative properties obtained when assuming the different dilectric mixing formula are of negligible importance with respect to the differences obtained using the diverse microphysical descriptions. Thus, for simplicity, only the Maxwell-Garnett mixing formula is assumed in the present study.

Scattering computations concerning the dry and mixed-phase aggregate obtained with the SAM model are performed using the ADDA ("Amsterdam DDA") code by *Yurkin and Hoekstra* [2011] which is a memory efficient implementation of the DDA methodology [*Penttila et al.*, 2007]. DDA is a numerical method for solving the integral volume equation of electromagnetic scattering, in which the scatterer is approximated by a set of polarizable points and can thus be applied to any shape. The accuracy of DDA is determined by the number of dipoles used to describe the shape of the scattering particle. To approximate homogeneous medium, the spacing d within the dipoles must be small relative to the wavelength; *Draine and Flatau* [1994] propose, as a rule of thumb for the correctness of the methodology, that $|n|kd \ll 1$ where k is the wave vector in the vacuum and n is the complex index of refraction of the medium. The correct representation of the target shape requires also that the dipole spacing must be smaller than any structural length of the target. In order to properly represent the hexagonal columns, which are the constituent particles of the simulated snow aggregates, a dipole spacing of 20 μm is used for the aggregates with D_{max} smaller than 13 mm and a dipole spacing of 40 μm for those with larger D_{max}. For this configuration, the maximum frequencies of the incoming electromagnetic wave allowed by the model are 660 GHz for the smallest particles and 330 GHz for the largest ones. The computed radiative properties, for all the simulations, are the total scattering cross section C_s, the total absorption cross section C_a and the radar backscattering cross section σ_{bk} . The radiative quantities are averaged over 1800 uniformly distributed orientations of the scattering particle.

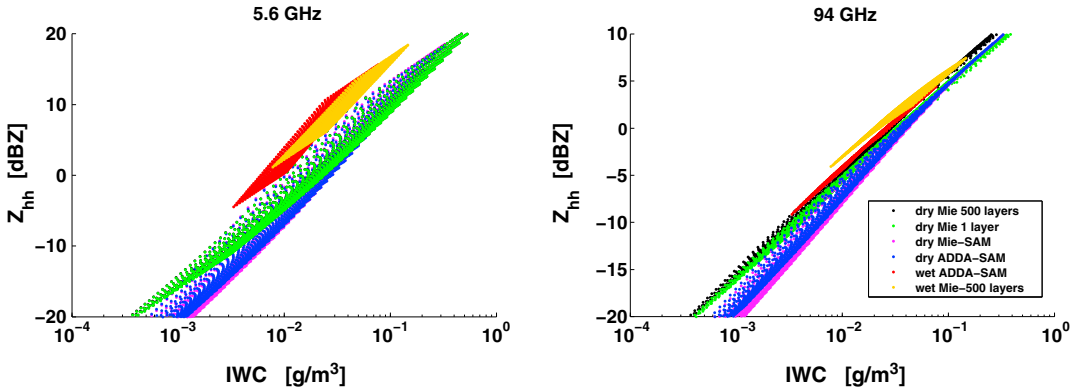

Figure 13. Copolar radar equivalent reflectivity at horizontal polarization for (left) C and (right) W frequencies as a function of IWC. Each dot is a computation of Z_{hh} for one of the 1632 PSD. Blue and red dots are obtained using ADDA-SAM for dry and mixed-phase particles (with 10% of melted mass), respectively; black and yellow dots are obtained for dry and wet Mie-500 layered sphere (with 10% of melted mass); green dots are obtained with the homogeneous Mie-1 models (in the left the black dots are completely overlapped by the green ones); magenta dots are obtained with the 50-layered Mie-SAM model (in both panels magenta dots are almost completely overlapped by the blue ones).

The DDA computational time increases as a power law with the target dimensions and as an exponential with the increase of the real part of the index of refraction of the material. Since the real part of the index of refraction of water is at least 2 times that of ice, over the spectrum range considered, the time required to complete DDA computation for partially melted snowflakes is much longer than that for equivalent dry particles. For this reason only one mixed-phase particle case is accounted for in the computations and the assumed melted fraction is set to 10%. The low fraction of liquid water allows to assume that the particle geometry is the same used for the dry snowflake.

3.2. Radiative Properties of Individual Particles

Figures 8 and 9 show respectively the total absorption and scattering cross section of the simulated aggregates, at two frequencies, as a function of the size parameter ($x = \pi D_{\max}/\lambda$) and compare these quantities with those derived for equivalent homogeneous and layered spheres.

The total scattering and absorption cross sections computed with Mie theory assuming one-layer homogeneous spheres or a 500 layered spheres, for particles with $D_{\max} < 3$ mm ($x = 1.1$ at 35.6 GHz and $x = 4.9$ at 157 GHz), show larger values than those computed for the complex aggregates with DDA model. The reason is related with the assumption made on the density distribution within the particle. As stated in section 2, the SAM model simulates complex-shaped particles with small dimensions that have smaller mass density than those predicted by equation (3). On the contrary, for particles modeled as soft spheres (one homogeneous layer) or 500 layered spheres (Mie-500 layers in the plots) it is assumed that the internal mass distribution follows exactly equation (3). That explains why the total scattering and absorption cross sections of the spherical models for small particles are larger than those computed with the complex aggregate models. This fact is confirmed by the comparison of the results of the ADDA-SAM model with those of the Mie-SAM model (solid magenta line) for which the density distribution is the same. The two models show closer computed scattering and absorption cross sections. The differences among results for the homogeneous spheres, the 500 layered spheres, and the 50 layered sphere Mie-SAM allow to evaluate the effect of the density distribution on main radiative properties.

For maximum dimensions larger than 5 mm ($x = 1.9$ at 35.6 GHz and $x = 8.2$ at 157 GHz) the total scattering cross section C_s computed for the aggregates with DDA model becomes larger than that computed for spheres with Mie theory (Figure 9); the differences are significantly larger in case of homogeneous sphere or 500 layered sphere. A similar behavior occurs for the total absorption cross section C_a but with lesser discrepancies (Figure 8). The differences are mainly related to the diverse microphysical structures of the particles produced by the considered models. In the SAM model the ice mass occupies only the volume defined by the pristine ice crystals that compose the aggregate, and the particle can be thought as a sum of discrete scatterers having dielectric constant of solid ice in a volume filled with air. In the soft-sphere and layered-sphere case the ice mass of the modeled snowflake is distributed in a spherical volume and in multiple spherical shells, respectively. The ice mass is diluted all over the volume, and the particle total

Table 2. Particle Size Distribution Parameters Adopted for the Computation of Dry and Wet Snow Equivalent Radar Reflectivity

Dry	Wet
$2.2 \leq \Lambda \leq 8.8$ mm^{-1}	$1.8 \leq \Lambda \leq 3.1$ mm^{-1}
$2,380 \leq N_0 \leq 42,000$ mm^{-1} m^{-3}	$1,515 \leq N_0 \leq 4,800$ mm^{-1} m^{-3}
$1.0 \leq D \leq 15.0$ mm	

density is lower than that of pure ice. The total dielectric properties of the spherical snowflake are obtained by a composition of the dielectric properties of ice with those of air that is supposed to be trapped in the spherical structure of the particle. As a consequence, the value of the index of refraction of the spherical target is closer to the value of the index of refraction of the air, and thus, the interaction with the incoming electromagnetic waves is less intense. This fact is more and more significant as the dimension increases.

The absorption and scattering cross sections calculated using the ADDA-SAM model are at about 30% larger than those obtained with the Mie-SAM model and are significant for all the investigated size parameters. Since these two models have the same radial mass distribution, the greater values of scattering and absorption cross sections for the ADDA-SAM models are imputable to the different microphysical structure.

Shape-dependent effects in the backscattering cross section σ_{bk} are encountered for size parameters larger than 2. Figure 10 shows the radar backscattering cross section σ_{bk} as a function of the snowflake size parameter at six different wavelengths. The backscattering cross section computed using the Mie theory presents the typical Mie resonance behavior that, otherwise, is strongly attenuated for results obtained using the ADDA-SAM model in case of aggregates. The backscattering cross section of complex aggregates shows only the first-order Mie resonance minimum, and this minimum is encountered for a larger size parameter with respect to that expected for the homogeneous soft sphere.

Comparing the results obtained from the soft-sphere and the layered-sphere models, the effect of the internal mass distribution of the particle on σ_{bk} can be evaluated. The modification of the Mie resonance structure of the layered-sphere model reflects the fact that in a layered sphere each layer is characterized by a proper refractive index and thus by a characteristic length for the backscattering resonance; the result is a composite contribution from each layer leading to a modification of the positions in the Mie's resonance minima typical of homogeneous spheres. The introduction of a stratified morphology with the layered-sphere model causes therefore the modification of the Mie's resonance structure. The ADDA-SAM model does not present a well-recognizable resonance behavior due to a lack of symmetry in the geometrical structure of the particle. Nevertheless, a singular minimum is still present when the size parameter is equal to 3.

The backscattering cross sections computed with the ADDA-SAM model is in good agreement with those obtained with the Mie-SAM model for size parameter smaller than about 3. This fact suggests that the radial mass distribution has a leading role on the determination of the backscattering cross section for this range of size parameters.

For particles with size parameter greater than 3, σ_{bk} computed with the ADDA-SAM model show increasing deviations (up to 3 orders of magnitude) from the results obtained with every assumed spherical approximation. The corresponding differences in the total scattering cross section are much smaller. The main parameter influencing the differences is the value of the phase function at 180°. Figure 11 (left) shows the value of the phase function at 180°, as a function of size parameter, computed for dry snowflakes at 94 GHz using the different models. In Figure 11 (right) the phase functions of particles with $D_{max} = 13$ mm at 94 GHz (corresponding to $x = 12.8$) are presented. Very large differences are encountered at the backscatter angle of 180° where the phase function computed for different models spans over about 5 orders of magnitudes. The larger values are found in case of ADDA-SAM model and are consistent with results shown in Figure 10.

The differences between the scattering properties at 35.6 and 94 GHz for mixed-phase particles and dry snowflakes are shown in Figure 12. Even if the melted fraction of the wet snowflake is only 10%, the scattering simulations show an increase in the total scattering cross section that is of the order of 30% to 50% with respect to the dry particle. The cross-section difference is larger for the lowest frequencies because the real part of the water refraction index at microwave increases as the frequency of the incoming electromagnetic wave decreases (Table 1). The partial melting of the snowflakes increases their effective refractive index. As a consequence, the positions of the resonance minima of the backscattering cross section, computed using the spherical models, shift to lower size parameters. This shift is responsible for the strong oscillating

behavior of the difference between the radar backscattering cross section of the wet and the dry particles for all the spherical models (bottom row of Figure 12). The difference between the scattering properties of mixed-phase particles and dry snowflakes is larger for the spherical models than for the ADDA-SAM model as a consequence of change in the effective refractive index of the overall spherical volume that is otherwise a localized effect in case of aggregate.

3.3. Scattering Properties of Snow Size Distributions

The equivalent copolar radar reflectivity Z_{hh} at each frequency is calculated by integrating the copolar radar backscattering cross section σ_{hh} as a function of the maximum particle size over the whole particle size distribution (PSD).

$$Z_{hh} = \frac{\lambda^4}{\pi^5 |K|^2} \int_{\min(D_{\max})}^{\max(D_{\max})} \sigma_{hh}(D_{\max}) N(D_{\max}) \mathrm{d}D_{\max} \tag{6}$$

In equation (6), λ is the wavelength, σ is the backscattering cross section, and $K = (n_w^2 - 1)/(n_w^2 + 2)$ is the dielectric factor (n_w is the complex index of refraction of water). Following *Straka et al.* [2000] it is assumed an inverse exponential PSD:

$$N(D) = N_0 \cdot e^{-\Lambda D}, \tag{7}$$

where the distribution parameters $N_0[\mathrm{mm}^{-1}\ \mathrm{m}^{-3}]$ and $\Lambda[\mathrm{mm}^{-1}]$ are derived from *Marzano et al.* [2007, 2010] and reported in Table 2 for dry and wet aggregate distributions.

The ice water content (IWC ($\mathrm{g/m^3}$)) can be expressed as

$$\mathrm{IWC} = \int_{\min(D_{\max})}^{\max(D_{\max})} m(D_{\max}) N(D_{\max}) \mathrm{d}D_{\max} \tag{8}$$

where $m(D_{\max})$ is the mass of the particles as a function of their maximum dimension (equation (3)) and $N(D_{\max})\mathrm{d}D_{\max}$ is the particle concentration within the size bin of width $\mathrm{d}D_{\max}$ around $D_{\max}$.

Z_{hh} and IWC are calculated for 1632 different PSDs. The PSD parameters used for these computations have been selected by uniformly sampling values between the parameter's limit expressed in Table 2. The numerical integration has been performed using the Simpson quadrature rule. The PSDs have been truncated at $\min(D_{\max}) = 1$ mm and $\max(D_{max}) = 15\ mm$ as in *Marzano et al.* [2010]. The results of these calculations are shown in Figure 13.

Z_{hh} of dry snowfall obtained from the radiative properties of the ADDA-SAM model and the Mie-SAM model (Figure 13) are very similar as a consequence of the relatively small differences in the computed σ_{bk}.

Z_{hh} of dry snowfall obtained from the scattering data of the ADDA-SAM model are lower than those obtained with the Mie-1 and Mie-500 layer models. The differences between the data sets are of the order of 5 dBZ for all the frequencies investigated and for values of IWC of the order of 10^{-4} $\mathrm{g/m^3}$ and reduces as the ice content increases. These differences at small values of IWC are mainly due to the features of the PSDs used for the comparisons. The inverse exponential PSD implies a large number of small particles. Since, for small particles, the sphere-Mie data sets show larger backscattering cross sections with respect to the ADDA-SAM model, larger reflectivity values are computed for distribution of spherical scatterers. As the PSD mean shifts to larger values the difference between the two data sets reduces due to the larger amount of large snowflakes included in the PSD. Note that aircraft measurements of the snow size distribution are generally affected by particles shattering at the optical probes [*Heymsfield et al.*, 2008] and the relative importance of small particles to the total reflectivity could be generally overestimated. For an unbiased calculation of the snow reflectivity it is thus necessary to properly represent both the particle's radiative properties and the PSD characteristics.

The difference between the ADDA-SAM and the Mie radar reflectivities in the case of wet snowflakes are of the order of 2 dBZ for all the frequencies. The reduced difference between the two data sets with respect to the dry case is explained by considering the fact that the difference of the backscattering cross section between wet and dry snowflakes for small particles (Figure 12) is larger in the spherical models than in the ADDA-SAM model.

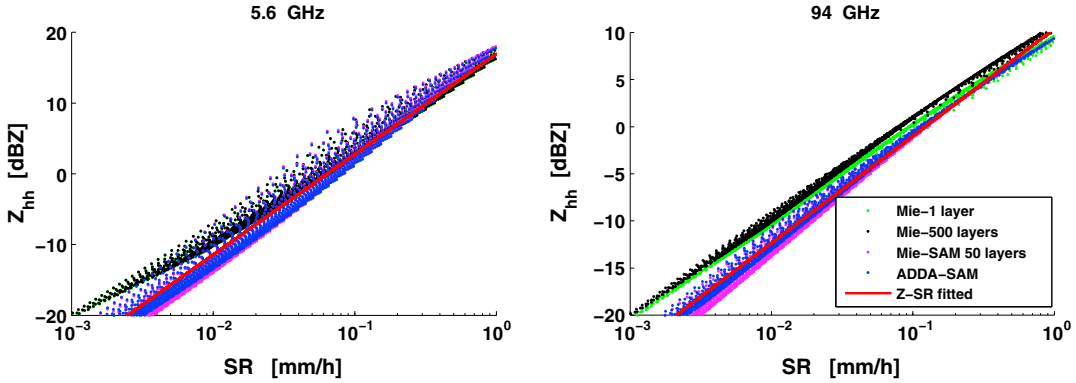

Figure 14. Copolar radar equivalent reflectivity at horizontal polarization for (right) C and (left) W frequency bands as a function of the snow rate. Each blue dot represent a different PSD of dry snow in the ADDA-SAM model. The overlapped red line is a power law fit of the results of the ADDA-SAM model. Black and green dots represents the results obtained using the Mie-1 homogeneous sphere and the Mie-500 layered-sphere models, respectively (in the left the green dots are completely overlapped by the black ones); magenta dots are obtained with the 50-layered Mie-SAM model (in both panels magenta dots are almost completely overlapped by the blue ones).

3.4. Snowfall Rate and Scattering Simulations

Liquid equivalent snowfall rate (SR) can be expressed as

$$\mathrm{SR} = \rho^{-1} \int_{\min(D_{\max})}^{\max(D_{\max})} m(D_{\max}) v_t(D_{\max}) N(D_{\max}) \mathrm{d}D_{\max} \tag{9}$$

where $m(D_{\max})$ is the mass size relation of the snowflakes (equation (3)), ρ is the mass density of water, and $v_t(D_{\max})$ is the terminal fall velocity-size relation. Equation (9) is expressed in general units of measure as in *Matrosov* [2007]; given units of measure for the operands used in the text (grams for masses, m/s for terminal fall velocities, $\mathrm{mm}^{-1}\ \mathrm{m}^{-3}$ for PSD, and millimeters for $D_{\max}$) a factor of 3.6e6 should be applied to convert the resulting m/s to the most commonly used mm/h.

The relationship between falling speed and size of snowflakes is a complicate relation of the type and shape (and other properties) of the snowflakes. Numerous studies have modeled the terminal fall velocity of aggregate snowflakes with a power law relationship as a function of the maximum dimension of the falling particle. The equations describing the falling speed as a function of the size of the snowflakes are just simplified formulas, and the accuracy of these relationships is not guaranteed. *Brandes et al.* [2007] published two speed-size relationships that come from fitting data sets from two different snow events:

$$\begin{aligned} v_t(D_{\max}) &= 2.076 D_{\max}^{0.141} \\ v_t(D_{\max}) &= 2.958 D_{\max}^{0.157} \end{aligned} \tag{10}$$

Another speed-size relation from *Straka et al.* [2000] is also introduced to evaluate the sensitivity of SR to the fall speed-size relation

$$v_t(D_{\max}) = 4.836 D_{\max}^{0.25} \tag{11}$$

For the three fall speed-size relations shown the $D_{\max}$ is expressed in meters. For particle dimension less than 5 mm (that represent the majority of the considered PSDs) equation (11) falls in between the two Brandes' relationships (equation (10)).

The Z_{hh}-SR relationships are particularly important because they give the opportunity to directly measure the amount of precipitation from radar measurements. Figure 14 shows the computed copolar reflectivity as a function of the sampled PSD for two radar frequencies. A power law's fit (red line) of the Z_{hh}-SR results is also shown in case of dry aggregates.

In C band the differences between the Z_{hh} computed with the homogeneous sphere model and the 500 layered-sphere model are minimal. The differences against ADDA-SAM results decrease from 2 to 0 dBZ as the liquid equivalent snowfall rate increases from 0.001 to 1 mm/h. As discussed in the previous section for

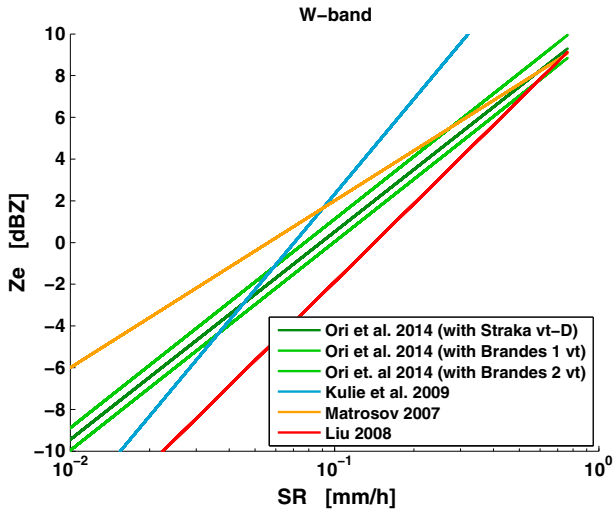

Figure 15. Various *Z*-SR relationships at W band are compared (see legend for the reference). The SAM aggregates *Z*-SR relation is evaluated for the different fall speed-size formulas.

the *Z*-IWC relations this characteristic is due to the relative importance of small particles in the used PSDs. For W band the reflectivity computed using the 500 layered-sphere model is 3 dBZ greater than that computed using the homogeneous sphere model. The ADDA-SAM results are equivalent to the homogeneous sphere results for liquid-equivalent snowfall rates of the order of 0.01 mm/h and become equivalent to those obtained with the 500 layered-sphere model for snowfall rates of the order of 1 mm/h. The Mie-SAM and ADDA-SAM computed Z_{hh} are very similar principally due to the large amount of small particles considered in the used PSDs. Size parameters larger than 5 are necessary to originate significant differences between the two models.

Given the importance of the *Z*-SR relation at W band, which is the frequency of the cloud profiling radar on board the CloudSat satellite, in Figure 15 the calculated *Z*-SR relationship derived for the aggregates (and using all the three fall speed-size relations discussed above) is compared to other results published in literature. This comparison shows that the sensitivity of the derived $Z - SR$ relationship to the assumed fall speed-size parametrization is much less than the spread observed for the other $Z - SR$ relationships.

4. Conclusions

A new approach (SAM) that generates realistic dry and mixed-phase snow particles is developed. The study aims at simulating physically based complex snowflake habits that follow measured size-mass relations. The model uses simple hexagonal columns with variable linear dimensions and random orientation as building blocks. The implemented aggregation process is sufficiently versatile to model the aggregation of crystals of arbitrary shapes and sizes, but the growth of the snowflakes is statistically constrained to follow a specified size-mass relationship [*Brandes et al.*, 2007]. The aspect ratios of the generated flakes have been analyzed to assess their consistency with the snowflakes observed by *Brandes et al.* [2007]. The fitting of a specific size-mass relation is just a demonstration of applicability of SAM. Future work will aim at model particles that fit different published mass-size relations in order to better represent the natural variability of snow characteristics. The modeling of melting snowflakes allows to simulate the transition from the radiative properties of a dry snowflake to those of a mixed-phase particle which are of primary importance for the remote sensing of midlatitude precipitation. A direct comparison of the single-scattering properties of dry and wet snowflakes with the same mass, dimension, and shape is performed. Since a relevant melting process would change the morphology of the snowflake, the proposed method is not appropriate to model mixed-phase particles with large values of melted fraction. Future work will focus on the representation of wet snow with any value of melted fractions.

The radiative properties of the simulated particles are computed using the DDA method at 7 frequencies. Results from the ADDA-SAM models are compared to those of simplified spherical objects computed using the Mie solution. Different levels of accuracy for the representation of the radial mass distribution of the spherical targets are adopted. The highest degree of approximation of the complex aggregate using the spherical assumption is obtained by modeling a layered sphere with the exact radial density distribution of the SAM snowflake. The comparison between the radiative quantities calculated with the different models addresses the problem of the determination of the range of applicability of the spherical approximation for the modeling of complex snowflakes in radiative transfer studies. The analysis of the radiative properties obtained with the spherical models and the complex aggregated particles produced by SAM shows that the former are inadequate to represent the scattering characteristics of large aggregated particles

(Figures 8 and 9). In particular, for size parameters larger than 3 the ADDA-SAM backscattering cross-section values are up to 3 orders of magnitude larger than those of spheres (Figure 10). Moreover, backscattering cross sections of the ADDA-SAM models do not show any strong resonance effect.

Large differences in the phase functions computed with ADDA-SAM or assuming a Mie-spherical model are observed. Otherwise, differences in the total scattering cross-sections are less significant.

The backscattering cross sections are integrated over a set of PSDs in order to evaluate the sensitivity of radar parameters to the different models of snowflakes. Substantial differences between the radiative properties calculated using complex models (such as ADDA-SAM) and those obtained from simplified spherical models (Mie applied to homogeneous sphere) are observed. However, when a Mie solution is applied to a layered-sphere model with same radial density distribution as the one obtained for the aggregates, differences in the Z_{hh} are much less intense for the PSDs considered. Calculations of the radar equivalent reflectivity are sensitive to the radar backscattering model as well as the mass-dimension relationship and the PSDs used to describe the precipitation. For this reason it is fundamental to develop a robust characterization of ice and snow microphysical properties based on observations in order to properly model the radiative properties of snowflakes and develop robust Z-SR relationships.

Given the generality of the collision-coalescence method of aggregation, the evolution of the SAM code is able to simulate the aggregation process of an entire population of pristine crystals which gives a physical link between the characteristics of the simulated aggregates and the thermodynamic variables of the environment.

Future investigation on hydrometeors with preferential orientation will allow a more complete study of the radar signature of snowfalls. Also, the study of radiative properties of snowflakes at higher frequencies will enhance the performance of snow detection algorithms allowing a better exploitation of passive MW radiometer's data and active/passive MW synergy, enhancing the exploitation of multifrequency radar and radiometer capabilities being deployed in future satellite missions.

Acknowledgments
All the reviewers provided many useful comments that substantially improved the quality of this work. All data used in this paper may be obtained by contacting the corresponding author.

References

Botta, G., and K. Aydin (2010), Modeling of microwave scattering from cloud ice crystal aggregates and melting aggregates: A new approach, *Geosci. Remote Sens. Lett.*, *7*(3), 572–576.

Brandes, A., K. Ikeda, G. Zhang, M. Schonhuber, and R. M. Rasmussen (2007), A statistical and physical description of hydrometeor distributions in Colorado snowstorms using a video disdrometer, *J. Appl. Meteorol. Climatol.*, *46*(5), 634–650, doi:10.1175/JAM2489.1.

Draine, B. (1988), The discrete dipole approximation and its application to interstellar graphite grains, *Astrophys. J.*, *333*, 848–872.

Draine, B., and P. Flatau (1994), Discrete-dipole approximation for scattering calculations, *J. Opt. Soc. Am. A*, *11*(4), 1491–1499.

Evans, K., and G. Stephens (1995), Microwave radiative transfer through clouds composed of realistically shaped ice crystals. Part I: Single scattering properties, *J. Atmos. Sci.*, *52*(11), 2041–2057.

Fabry, F., and W. Szyrmer (1999), Modeling of the melting layer. Part II: Electromagnetic, *J. Atmos. Sci.*, *56*, 3593–3600.

Grecu, M., and W. Olson (2008), Precipitating snow retrievals from combined airborne cloud radar and millimeter-wave radiometer observations, *J. Appl. Meteorol. Climatol.*, *47*, 1634–1649, doi:10.1175/2007JAMC1728.1.

Heymsfield, A., A. Bansemer, C. Schmitt, C. Twohy, and M. Poellot (2004), Effective ice particle densities derived from aircraft data, *J. Atmos. Sci.*, *61*, 982–1003.

Heymsfield, A., P. Field, and A. Bansemer (2008), Exponential size distributions for snow, *J. Atmos. Sci.*, *65*, 4017–4031.

Holroyd, E. W., III (1971), The meso- and microscale structure of Great Lakes snowstorm bands: A synthesis of ground measurements, radar data, and satellite observations, PhD dissertation, 148 pp., State Univ. of New York at Albany, N. Y.

Hong, G. (2007a), Parameterization of scattering and absorption properties of nonspherical ice crystals at microwave frequencies, *J. Geophys. Res*, *112*, D11208, doi:10.1029/2006JD008364.

Hong, G. (2007b), Radar backscattering properties of nonspherical ice crystals at 94 GHz, *J. Geophys. Res.*, *112*, D22203, doi:10.1029/2007JD008839.

Ishimoto, H. (2008), Radar backscattering computations for fractal-shaped snowflakes, *J. Meteorol. Soc. Jpn.*, *86*(3), 459–469.

Kim, M., M. Kulie, C. O'Dell, and R. Bennartz (2007), Scattering of ice particles at microwave frequencies: A physically based parameterization, *J. Appl. Meteorol. Climatol.*, *46*, 615–633.

Kneifel, S., U. Löhnert, A. Battaglia, S. Crewell, and D. Siebler (2010), Snow scattering signals in ground based passive microwave radiometer measurements, *J. Geophys. Res.*, *115*, D16214, doi:10.1029/2010JD013856.

Korkmaz, S. (2004), Radar attenuation due to melting: A comparison of physical models proposed for the melting morphology, *Atmos. Res.*, *70*, 261–274, doi:10.1016/j.atmosres.2004.01.005.

Korolev, A., G. Isaac, S. Cober, J. Strapp, and J. Hallett (2003), Microphysical characterization of mixed-phase clouds, *Q. J. R. Meteorol. Soc.*, *129*, 39–65.

Kulie, M., R. Bennartz, T. Greenwald, Y. Chen, and W. Fuzhong (2010), Uncertainties in microwave properties of frozen precipitation: Implications for remote sensing and data assimilation, *J. Atmos. Sci.*, *67*, 3471–3487.

Leinonen, J., S. Kneifel, D. Moisseev, J. Tyynela, S. Tanelli, and T. Nousianen (2012), Evidence of nonspheroidal behavior in millimeter-wavelength radar observations of snowfall, *J. Geophys. Res.*, *117*(D18), D18205, doi:10.1029/2012JD017680.

Liu, G. (2004), Approximation of single scattering properties of ice and snow particles for high microwave frequencies, *J. Atmos. Sci.*, *61*, 2441–2456.

Liu, G. (2008a), A database of microwave single-scattering properties for nonspherical ice particles, *Bull. Am. Meteorol. Soc.*, 1563–1570, doi:10.1175/2008BAMS2486.1, (to appear in print).
Locatelli, J., and P. Hobbs (1974), Fall speeds and masses of solid precipitation particles, *J. Geophys. Res.*, *79*(15), 2185–2197.
Löhnert, U., S. Kneifel, A. Battaglia, M. Hagen, L. Hirsch, and S. Crewell (2011), A multisensor approach toward a better understanding of snowfall microphysics: The TOSCA project, *Bull. Am. Meteorol. Soc.*, *92*, 613–628.
Magono, C., and C. Lee (1966), Meteorological classification of natural snow crystals, *J. Fac. Sci. Kokkaido Univ.*, *2*(4), 321–366.
Marzano, F., D. Scaranari, and G. Vulpiani (2007), Supervised fuzzy-logic classification of hydrometeors using C-band weather radars, *Trans. Geosci. Remote Sens.*, *45*(11), 3784–3799.
Marzano, F., G. Botta, and M. Montopoli (2010), Iterative Bayesian retrieval of hydrometeor content from X-band polarimetric weather radar, *Trans. Geosci. Remote Sens.*, *48*(8), 3059–3074.
Matrosov, S. (2007), Modeling backscattering properties of snowfall at millimeter wavelengths, *J. Atmos. Sci.*, *64*, 1727–1736, doi:10.1175/JAS3904.1.
Matzler, C. (2006), *Thermal Microwave Radiation: Applications for Remote Sensing,* IET Electromagnetic Waves Series, London, U. K.
Meissner, T., and F. Wentz (2004), The complex dielectric constant of pure and sea water from microwave satellite observations, *Trans. Geosci. Remote Sens.*, *42*(9), 1836–1849.
Mishchenko, M. I., L. D. Travis, and D. W. Mackowski (1996), T-matrix computations of light scattering by nonspherical particles: A review, *J. Quant. Spectrosc. Radiat. Transfer*, *55*, 535–575, doi:10.1016/0022-4073(96)00002-7.
Mitchell, D. (1996), Use of mass- and area-dimensional power laws for determining precipitation particle terminal velocities, *J. Atmos. Sci.*, *53*(12), 1710–1723.
Nowell, H., G. Liu, and R. Honeyager (2013), Modeling the microwave single-scattering properties of aggregate snowflakes, *J. Geophys. Res. Atmos.*, *118*, 7873–7885, doi:10.1002/jgrd.50620.
Oraltay, R., and J. Hallett (2005), The melting layer: A laboratory investigation of ice particle melt and evaporation near 0C, *J. Appl. Meteorol. Climatol.*, *44*, 206–220.
Osharin, A. M. (1994), Millimeter-wave scattering by dry snow crystals, *Radiophys. Quantum Electron.*, *37*(11), 924–930.
Pena, O., and U. Pal (2009), Scattering of electromagnetic radiation by a multilayered sphere, *Comput. Phys. Commun.*, *180*, 2348–2354.
Penttila, A., E. Zubko, K. Lumme, K. Muinonen, M. Yurkin, B. Draine, J. Rahola, A. Hoekstra, and Y. Shkuratov (2007), Comparison between discrete dipole implementations and exact techniques, *J. Quant. Spectrosc. Radiat. Transfer*, *106*, 417–436.
Petty, G., and W. Huang (2010), Microwave backscatter and extinction by soft ice spheres and complex snow aggregates, *J. Atmos. Sci.*, *67*, 769–787.
Straka, J., D. Zrnic, and A. Ryzhkov (2000), Bulk hydrometeor classification and quantification using polarimetric radar data: Synthesis of relations, *J. Appl. Meteorol. Climatol.*, *39*, 1341–1372.
Taflove, A., and S. Hagness (2005), *Computational Electrodynamics: The Finite-Difference Time-Domain Method,* 3rd ed., Artech House, Norwood, Mass.
Tyynela, J., J. Leinonen, D. Moisseev, and T. Nousianen (2011), Radar backscattering from snowflakes: Comparison of fractal, aggregate, and soft spheroid models, *J. Atmos. Oceanic Technol.*, *28*, 1365–1372.
Yang, W. (2003), Improved recursive algorithm for light scattering by a multilayered sphere, *Appl. Opt.*, *42*(9), 1710–1720.
Yurkin, M., and A. Hoekstra (2011), The discrete-dipole-approximation code ADDA: Capabilities and known limitations, *J. Quant. Spectrosc. Radiat. Transfer*, *112*, 2234–2247.